A tandem photoelectrochemical cell based on Cu2-xTe nanocrystals for solar energy conversion to hydrogen

Solar Energy Materials & Solar Cells 250 (2023) 112050

Contents lists available at ScienceDirect

Solar Energy Materials and Solar Cells

journal homepage: www.elsevier.com/locate/solmat

A tandem photoelectrochemical cell based on $Cu_{2-x}Te$ nanocrystals for solar energy conversion to hydrogen

Elena Alfonso-González [a], Marta Liras [a], Mengjiao Wang [b], Ignacio J. Villar-García [a,1], Luca de Trizio [b], Mariam Barawi [a,*], Victor A. de la Peña O'Shea [a,**]

[a] Photoactivated Processes Unit, IMDEA Energy Institute, Avda. Ramón de la Sagra 3, 28935, Móstoles, Madrid, Spain
[b] Nanochemistry Department, Istituto Italiano di Tecnologia, Via Morego 30, 16163, Genova, Italy

A B S T R A C T

In this work we present the design, assembly and characterization of a tandem photoelectrochemical (PEC) cell based on two different crystallographic phases of sub-stoichiometric copper telluride nanocrystals (NCs). The first one, a pseudo-cubic phase, pc-$Cu_{2-x}Te$, is characterized by positive photocurrents, while the second one, a hexagonal phase, h-$Cu_{2-x}Te$, favors negative ones. Taking advantage of the different optoelectronic properties of the two $Cu_{2-x}Te$ structures, we prepared a PEC cell composed of a hybrid pc-$Cu_{2-x}Te/TiO_2$ photoanode, with TiO_2 acting as a light absorber and electron selective layer, and a h-$Cu_{2-x}Te$/CuI photocathode, with CuI behaving as a photo-absorber and hole selective layer. The tandem PEC cell shows a photocurrent density of ~0.5 mA/cm^2 when measured in a 2-electrode configuration without any co-catalyst. Finally, to test the PEC cell performance for the hydrogen evolution reaction (HER), a thin film of Pt was deposited on top of the photocathode and ~7 μmol of hydrogen were obtained at 0.6 V in a 1-h experiment, reaching a photocurrent of 1 mA/cm^2 with no losses.

1. Introduction

Looking at the ever-increasing global energy demand and the undesirable environmental impact of fossil fuels, solar energy emerges as an alternative green source because of its abundance and renewable nature [1,2]. While the conversion of such energy into electricity *via* solar cells is a highly studied and efficient process, the storage of the generated electric energy remains a bottleneck due to the lack of effective accumulators/batteries. A direct use of the solar energy to obtain fuels via artificial photosynthesis is a very promising approach [3]. In this context, photoelectrochemical (PEC) cells are one of the most attractive technologies, as they have led to some of the highest solar-to-hydrogen efficiencies achieved to date [4]. In a typical PEC system, one or both (tandem PEC cell) of the two electrodes are used to harvest solar radiation, acting as a photoanode where holes are the minority carriers that carry out the oxidation reaction or as a photocathode where electrodes are the minority carriers that carry out the reduction reaction.

The principal requirements to choose a material for this application are the ability to absorb solar energy irradiance and to have a suitable electronic structure that provides electrons and holes capable of carrying out the targeted oxidation and reduction reactions. In the case of the water splitting reaction, the position of the conduction band should be more negative than the H^+/H_2 potential, (0.0 V vs RHE), and the valence band more positive than the O_2/H_2O potential (1.23 V vs RHE). In this sense, many different materials have been investigated, with metal oxides being the most used by far [5–8], followed by metal chalcogenides [9,10]. Until now, the efficiency of these materials as photoelectrodes has mainly been hindered by low light absorption range, high charge recombination, limited chemical stability or a combination of the three [6,11]. Different strategies have been used to address these inefficiencies, such as doping, nanostructuring and the use of multinary metal oxides or smaller band gap materials such as some metal chalcogenides like CuSe, PbSe or HgSe [3,12–15]. However, until now no single material has been able to overcome all the main challenges described above [16]. Consequently, the latest approaches use a combination of materials in order to optimize the performance of each photoelectrode and maximize the efficiency of the final PEC. Advanced inorganic colloidal nanocrystal (NC) approaches to produce homogenous inks are some of the most interesting strategies to design efficient inexpensive photoelectrodes with a large surface area [17,18]. Colloidal synthesis approaches also allow to obtain a huge number of multifunctional and versatile materials with a high control over the size, size distribution, shape, composition, and surface termination [19–21].

* Corresponding author.
** Corresponding author.
E-mail addresses: mariam.barawi@imdea.org (M. Barawi), victor.delapenya@imdea.org (V.A. de la Peña O'Shea).
[1] Present address: ALBA Synchrotron, Carrer de la Llum 2–26, 08290, Cerdanyola del Vallès (Barcelona) Spain.

https://doi.org/10.1016/j.solmat.2022.112050
Received 22 June 2022; Received in revised form 16 September 2022; Accepted 6 October 2022
Available online 25 October 2022

These features, in turn, govern their optoelectronic properties and, consequently, their use as building materials for PEC cells [22–24]. Many colloidal systems have been employed in PEC cells [14,25–27] and among them, metal chalcogenides exhibit several advantages in comparison to metal oxides, such as higher conduction band edge positions, smaller band gap energy and greater conductivities [21,25,28]. In this regard, CdS and CdSe are among the most active materials for photocatalytic applications [25,28]. However, their low stability towards corrosion and the toxic and carcinogenic nature of cadmium represent a considerable hurdle for their widespread application. Consequently, other non-toxic and more stable metal chalcogenides are currently investigated as alternatives for the Hydrogen Evolution Reaction (HER) in PEC systems [29].

Over the past few years, copper chalcogenides, $Cu_{2-x}Y$ (Y = S, Se, Te), have generated much interest in photovoltaic, photonic and electrocatalytic applications due to their interesting opto-electronic properties and the high abundance and non-toxicity of copper [21,30,31]. These materials are characterized by the presence of copper vacancies which act as dopants, leading to the formation of free holes in the top of the valence band with a charge carrier density up to 10^{21} cm^{-3} [30]. Such free carriers also originate a strong localized surface plasmonic response falling in the near infrared region of the spectrum [30], increasing the amount of solar energy that can be collected. Among $Cu_{2-x}Y$ compounds, $Cu_{2-x}Te$ is characterized by the largest carrier mobility, due to the fact that Te is less electronegative than S and Se, and, therefore, Cu–Te bonds have the lowest ionic character (more covalent) and should, therefore, have a larger carrier mobility [21]. Several authors have shown a relationship between optical and electronic properties, such as band gap, conductivity, mobility and carrier concentration, with structural ones [32,33]. In fact, among the possible crystal phases, hexagonal $Cu_{2-x}Te$ has recently been studied as an electrocatalyst for HER, showing a low overpotential, very low charge transfer resistance, R_{ct}, and long-term stability [31]. However, as far as we know, $Cu_{2-x}Te$ has not been used as a photoelectrode material despite its potential due to their interesting optoelectronic properties. Motivated by such potential we decided to exploit the promising features of $Cu_{2-x}Te$ to build PEC cells. Specifically, we first synthesized colloidal $Cu_{2-x}Te$ NCs in hexagonal (h) and pseudo-cubic (pc) crystalline structures and characterized their optoelectronic and photoelectrochemical properties. We then employed these two materials to build a tandem PEC cell for HER in which h-$Cu_{2-x}Te$ NCs were used to build the photoanode and pc-$Cu_{2-x}Te$ NCs the photocathode. The resulting cell composed of two hybrid photoelectrodes is capable of generating ~7 μmol of hydrogen for 1 h under irradiation and the application of 0.6 V.

2. Materials and methods

2.1. Chemicals

Copper(II) acetylacetonate [$Cu(acac)_2$, 97%], trioctylphosphine oxide (TOPO, 99%), oleylamine (OAm, 70%), ethanol (anhydrous, ≥99.8%), chloroform (anhydrous, ≥99%), lithium bis(trimethylsilyl) amide ($LiN(SiMe_3)_2$, 97%), tri-*n*-octylphosphine (TOP, 97%) and 1-octadecene (ODE, 90%) were purchased from Sigma-Aldrich. Tellurium powder (Te, 99.999%) was purchased from Strem Chemicals. TOP, $LiN(SiMe_3)_2$ and tellurium powder were stored in a N_2 filled glovebox. All the chemicals were used as received.

2.2. Synthesis of $Cu_{2-x}Te$ NCs

$Cu_{2-x}Te$ NCs were synthesized following the procedure reported by Tu et al. [34] Typically, 0.655 g of $Cu(acac)_2$ and 3.866 g of TOPO were mixed with 50 mL of OAm in a 250 mL round bottom flask with electromagnetic stirring. The mixture was degassed under vacuum at 120 °C for 1 h to remove moisture and oxygen. Meanwhile, 2.5 mmol of Te powder were mixed with 1.25 mL of TOP and the resulting mixture was stirred at 150 °C for 2 h to form Te-TOP stock solution. Another transparent solution of 2.5 mmol of $LiN(SiMe_3)_2$ in 5 mL of ODE was prepared by sonicating the mixture at room temperature for 20 min. After degassing, the temperature was raised to 160 °C and 1.5 mL of TOP was injected firstly under a flow of Ar, then the as-prepared Te-TOP solution and the $LiN(SiMe_3)_2$ solution were injected. The mixture was heated to 220 °C and maintained at that temperature for 30 min under stirring. The product was cleaned twice by redispersion in chloroform and precipitation by the addition of ethanol. Eventually, the product was dispersed in toluene and stored in a N_2 atmosphere for further use. Nanoparticles are surrounded by trioctylphosphine oxide (TOPO) and oleylamine, to prevent the aggregation of NCs. These capping surfactants reduce the electrical conductivity and thus hinder the use of $Cu_{2-x}Te$ as photoelectrodes, as measured by electrochemical impedance spectroscopy (EIS) (Fig. S2 and Table S1). These capping agents were removed by a ligand exchange method using mercaptopropionic acid based on the one by Shuzo Tokumitsu [35].

2.3. Photoelectrodes preparation

To prepare the photoelectrodes, two aliquots of 15 μL of a 0.05 L/L ligand exchange solution (details in S. I) were deposited by drop casting on CuI or TiO_2 photoelectrodes or on bare ITO coated glass using a tape mask of 1 cm^2. Then, pc-$Cu_{2-x}Te$ photoelectrodes were heated at 150 °C for 1 h in an inert atmosphere in order to remove mercaptopropionic acid. To obtain h-$Cu_{2-x}Te$, pc-$Cu_{2-x}Te$ photoelectrodes were heated in an Ar atmosphere at 425 °C for 1 h.

The CuI thin film on the photocathodes was deposited by spin coating on functionalized ITO coated glass. First, 40 μL of triethylamine were spun at 800 rpm for 1 s and at 1600 rpm for 30 s for the functionalization of the substrate. Then, 80 μL of a CuI suspension 10 g/L in acetonitrile was spun at 1200 rpm for 3 s and at 2400 rpm for 60 s. The TiO_2 anatase film on the photoanode was prepared by doctor blade using Dye Sol DSL 18 NR-T TiO_2 paste, calcined at 500 °C for 1 h. The Pt thin film for HER quantification was deposited with an Agar manual sputter coater for 75 s.

2.4. Transmission electron microscopy (TEM)

The colloidal NCs were dispersed in toluene for the sample preparation. The samples were prepared by dropping diluted solutions of NCs onto carbon film-coated 200 mesh copper grids for TEM characterization. The TEM measurement was carried out on a JEOL JEM-1011 transmission electron microscope operating at an acceleration voltage of 100 kV.

2.5. Theoretical calculations

Theoretical calculations by periodic density functional theory (DFT) were carried out using a pseudocubic $Cu_{2-x}Te$ (x = 0.5) structure with 220 atoms. Geometry and electronic structure were performed using the projected augmented wave method implemented in Viena ab initio simulation package (VASP) [36,37], using the spin polarized version of the Perdew−Burke−Ernzerhof (PBE) [38]. The Heyd-Scuseria-Enzerhof hybrid functional (HSE06) [39], with a mixing parameter of 0.25, was used to fit a more accurate energy gap. The cut-off for the kinetic energy of the plane-waves was set to 500 eV to ensure a total energy and force convergence better than 10^{-4} eV and 0.01 eV/Å^3 respectively.

2.6. X-ray powder diffraction (XRD)

XRD patterns were acquired with a Bruker D8 Advance A25 diffractometer using Cu radiation from a Siemens type KFL Cu 2 K tube and operating with a Lynxeye XE detector. Colloidal $Cu_{2-x}Te$ was deposited on a silicon substrate and allowed to dry before measurements. The XRD chamber was heated in an Ar atmosphere and

diffractograms were recorded every 25 °C up to 500 °C, with a heating rate of 5 °C/min and steady temperature during XRD measurements.

2.7. Optical measurements

In order to avoid the interference of ITO in the signals, $Cu_{2-x}Te$ was deposited on bare glass substrates. Transmission and reflectance spectra were acquired with a PerkinElmer Lambda 1050 UV-VIS-NIR Spectrometer. Infrared spectra were recorded on a Thermo Scientific Nicolet 6700 FT-IR. A Park XE-100 microscope in non-contact mode was used to make AFM measurements, with a NSG30 cantilever from NT-MDT.

2.8. X-ray photoelectron spectroscopy (XPS)

XPS spectra were recorded using a SPECS NAP-XPS system incorporating the DeviSim NAP reaction cell. The spectrometer is equipped with an Al Kα monochromated source (hν = 1486.6 eV), composed of a SPECS XR50 MF x-ray gun and a μ-FOCUS 600 monochromator, and PHOIBOS 150 NAP 1D-DLD analyser. X-ray gun power was set to 25 W (1.68 mA emission current and 15 kV). With this X-ray settings, the intensity of the Ag 3d5/2 photoemission peak for an Ag sample, recorded at 10 eV pass energy (PE), was 1 × 104 cps and the full width at half maximum (FWHM) was 0.60 eV. Binding energy calibration was made using Au 4f7/2 (84.01 eV), Ag 3d5/2 (368.20 eV) and Cu 2p3/2 (932.55 eV). Each sample was analysed at an electron take-off angle normal to the surface with respect to the analyser. All high resolution scans presented in the manuscript and in the SI (Cu 2p, Te 3d and valence band) were taken using 10 eV pass energy (PE) and an energy step of 0.1 eV.

2.9. Photoelectrochemical (PEC) measurements and H_2 quantification

Photocurrent measurements of each photoelectrode were recorded in a three-electrode configuration cell with a quartz window using a Pt wire as counter electrode and an Ag/AgCl reference electrode in aqueous Na_2SO_3 0.5 M as the electrolyte solution. The tandem monolithic PEC cell was tested in a two-electrode configuration in aqueous Na_2SO_3 0.5 M. In both cases, Ar flowed continuously into the cell (10 mL min^{-1} for general characterization and 50 mL min^{-1} for H_2 quantification) and the electrolyte was purged before measurements. The light source was a LOT Quantum Design solar simulator equipped with a 300 W Xe lamp and an AM 1.5 G solar filter.

3- Results and discussion

Colloidal pc-$Cu_{2-x}Te$ nanocubes (see TEM image in Fig. 1a) where synthetized using a microemulsion method, based on the use of specific ligands (Trioctylphosphine oxide and Oleamine) as surfactants [30]. These NCs crystallize in the pseudo-cubic $Cu_{1.5}Te$ structure (Fig. 1b) characterized by the presence of Cu vacancies, as studied by Mugnaioli et al. (ref 30). Density-functional theory (DFT) calculations (Fig. 1c) were performed of the pseudo-cubic structure $Cu_{2-x}Te$ (x = 0.5) (further details in the supporting information, SI) to predict the electronic structure. The electronic density of states (DOS) of the pc-$Cu_{2-x}Te$ phase shows a valence band maximum (VBM) and a conduction band minimum (CBM) mainly composed of Cu 3d and Te 5d states. The presence of Cu vacancies leads to the appearance of electronic states above E_F. In addition, the electronic localization function (ELF) exhibits an increase in the electron density in the Te atoms next to a Cu vacancy (white arrow), while in the case of full coordinated Te atoms (red arrow) the electronic density is more homogeneous (Fig. 1d). This electronic configuration provides the material with a band gap energy of 1.68 eV, which is in good agreement with the optical one (see below). This small band gap will allow the material to absorb a wide range of the solar spectrum.

Colloidal solutions are ideal to produce homogenous thin films. However, they require a post-treatment to get rid of the ligand in order to improve conductivity of the resulting film. The original long-chain capping agents require a heating treatment well above the decomposition temperature of the CuTe material. Therefore, we performed a ligand exchange procedure [35] in order to replace the original long-chain capping agents with the shorter-chain mercaptopropionic acid. This ligand has a lower boiling point, below the temperature at which pc-$Cu_{2-x}Te$ NCs are unstable. The removal of the organic capping was monitored by FTIR (Fig. S1) and the effect of the ligand exchange

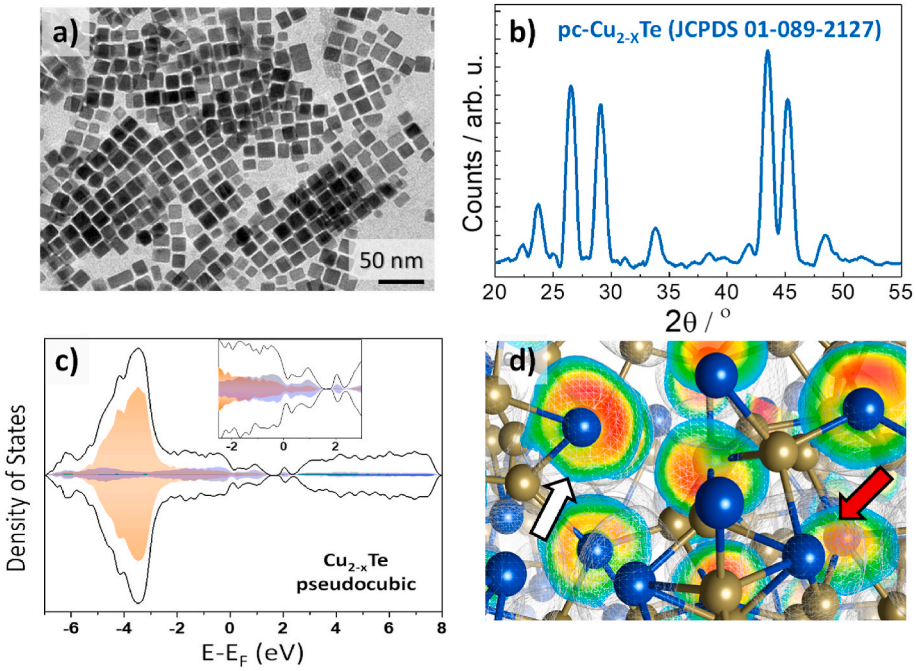

Fig. 1. a) TEM image of pc-$Cu_{2-x}Te$ NCs nanocubes, b) XRD diffractogram c) Projected Cu 3d (orange) and Te 5p (blue) density of states (DOS) with valence band (VB) magnification (inset) and d) electron localization function (ELF) of $Cu_{2-x}Te$ pseudo-cubic phase. The red color indicates that highest values and blue one the lowest. Atom color: Cu (gold) and Te (blue). (For interpretation of the references to color in this figure legend, the reader is referred to the Web version of this article.)

procedure was monitored by measuring the conductivity of the NCs film by Electrochemical Impedance Spectroscopy (EIS) (Fig. S2 and Table S1).

In order to prepare the photoelectrodes, the freshly produced ligand exchange colloidal solution ($Cu_{2-x}Te$ NCs dispersed in hexane) was deposited onto an Indium Tin Oxide (ITO) coated glass by drop casting (SI). We also prepared hexagonal (h) $Cu_{2-x}Te$ NCs via annealing of pc-$Cu_{2-x}Te$ thin films. The pc→h structure transition was studied by High Temperature X-Ray Diffraction (HT-XRD), monitoring the XRD patterns obtained when annealing pc-$Cu_{2-x}Te$ NCs from 25 °C to 500 °C under an argon flow (Fig. S3). At 300 °C we started to observe a mixture of pc and h phases, while a complete transition to the hexagonal phase occurred only at 425 °C, which changes slightly after cooling down, obtaining a weissite hexagonal crystal phase (Fig. S3). Moreover, after all the chemical and thermal treatments, we performed a XPS analysis of the films. Cu $2p_{3/2}$ and Te $3d_{5/2}$ XPS spectra in Fig. S4 show that even the photoelectrodes surface is mainly composed of CuTe in both films with an amount of oxide peaks being somewhat larger, as expected, for the case of the sintered sample at a higher temperature, h-$Cu_{2-x}Te$. Figs. S5–S8 exhibit the FESEM images and the cross section of the thin film of both crystallographic phase photoelectrodes, revealing a thickness of ~350 nm for pc-$Cu_{2-x}Te$ and ~100 nm for h-$Cu_{2-x}Te$.

The optoelectronic properties of both pc-$Cu_{2-x}Te$ and h- $Cu_{2-x}Te$ NC films were studied via optical, electronic and photoelectrochemical characterizations. Optical band gap energies were determined by means of UV-VIS-NIR transmittance and reflectance spectroscopy (Fig. S9). In this regard, the absorption coefficients were calculated (equation S1) and the corresponding Tauc plots were built. As can be seen in Fig. 2a and b, both crystal structures are characterized by a direct band gap of 1.68 eV for h-$Cu_{2-x}Te$ and 1.66 eV for pc-$Cu_{2-x}Te$. The band gap of pc-$Cu_{2-x}Te$ is similar to the value obtained from the DFT studies (1.68 eV, Fig. 1). The electronic band structure of both $Cu_{2-x}Te$ phases was experimentally obtained by the combination of several characterization techniques. The valence band (VB) energy determined by XPS is 0.11 ± 0.02 and 0.33 ± 0.02 eV for the pseudo-cubic and hexagonal phases, respectively (Fig. 2 c and d). These values, much lower than the band gap energy, indicate that both $Cu_{2-x}Te$ structures are p-type semiconductors, in agreement with what has been reported in literature [21]. Flat band potentials (V_{fb}), from which the Fermi level energy can be directly obtained [40], are −0.18 ± 0.02 and −0.12 ± 0.02 $V_{Ag/AgCl}$ at pH = 9 for pseudo-cubic and hexagonal phases respectively, as measured by linear sweep voltammetry (LSV) under dark and light conditions (Fig. S10). These correspond to 0.53 and 0.61 V vs RHE respectively. Additionally, the chronoamperometries performed under chopped illumination at different bias potentials confirm the photocurrent sign change (Fig. S11) and the ability of these materials to be used as photoelectrodes. The similar band gap and valence band positions obtained for both samples suggests that the vacancies identified in the DFT calculations must be also present in the h-$Cu_{2-x}Te$ sample. The small difference in valence band position indicates that the amount of vacancies must be slightly lower for the hexagonal phase.

Moreover, the conduction bands edges of both materials are more negative than the redox par responsible of the water reduction (see Fig. 2e) in the used pH electrolyte (pH = 9). The combination of these band positions and the optoelectronic properties of both crystal phases make them suitable to be part of a tandem cell for HER.

Photocurrents of both $Cu_{2-x}Te$ NC samples were then more exhaustively investigated at different bias potentials by chronoamperometries under chopped AM 1.5G illumination in the presence of Na_2SO_3 as sacrificial agent (0.5 M; pH = 9). Fig. 3a–b displays the anodic measurements, whereas the cathodic ones are shown in Fig. 3c–d. Fig. 3e exhibits the photocurrent values obtained at the different applied potentials. Interestingly, these measurements reveal that the pc-$Cu_{2-x}Te$ phase offers higher positive photocurrents than the h-$Cu_{2-x}Te$ phase, while the h-$Cu_{2-x}Te$ phase shows higher negative photocurrents than the pc-$Cu_{2-x}Te$ phase.

Besides, in the chronoamperometries of Fig. 3a we can see a current drop in the photocurrent after illuminating the pc-$Cu_{2-x}Te$ photoelectrode under negative bias that can be attributed to recombination and was also observed in h-$Cu_{2-x}Te$ in a smaller proportion. In order to elucidate this point and to investigate the charge transfer across the $Cu_{2-x}Te$/electrolyte interface, we performed EIS experiments (see Nyquist plot in Fig. 3f). By fitting the Nyquist plot, the equivalent electrical circuit was obtained. R_{ct} is the resistance associated with the electronic transport through the semiconductor-electrolyte interface. Its calculated values show better conductivity in pc-$Cu_{2-x}Te$ compared to h-$Cu_{2-x}Te$ (Table S1), which is in agreement with the highest photocurrents of the first at positive potentials. R_{ct} decreases considerably under illumination conditions, demonstrating the ability of these materials to be used as photoelectrodes in solar energy conversion.

Taking into account the optoelectronic properties and the photoelectrochemical response of both materials, we decided to design a multilayer 2-electrode tandem PEC cell where the photoanode was comprised of a combination of TiO_2 anatase and pc-$Cu_{2-x}Te$ NCs and the photocathode of CuI and h-$Cu_{2-x}Te$ NCs layers (Figs. S12 and S13 exhibit the electrodes cross section). TiO_2 is a well-known semiconductor used in photoanodes due to its low cost, very good chemical and optical stability [41,42]. Having TiO_2 a wide bandgap (*i.e.*, transparent in the

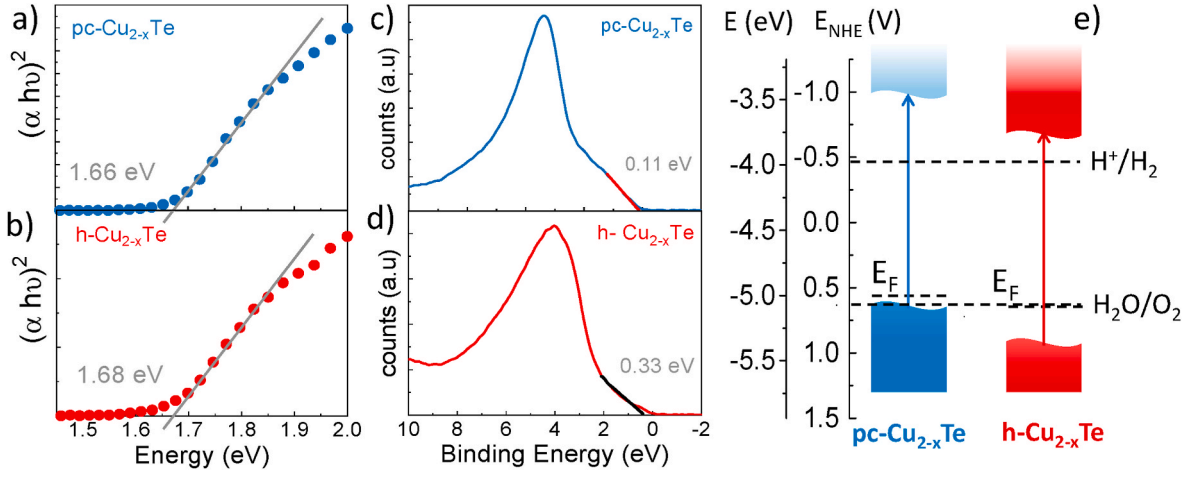

Fig. 2. a, b) Tauc plots obtained by UV-VIS-NIR Spectroscopy, c-d) XPS valence band spectra (see experimental section for XPS acquisition settings) and e) electronic band diagram of pc-$Cu_{2-x}Te$ (blue) and h-$Cu_{2-x}Te$ (red) at pH = 9. (For interpretation of the references to color in this figure legend, the reader is referred to the Web version of this article.)

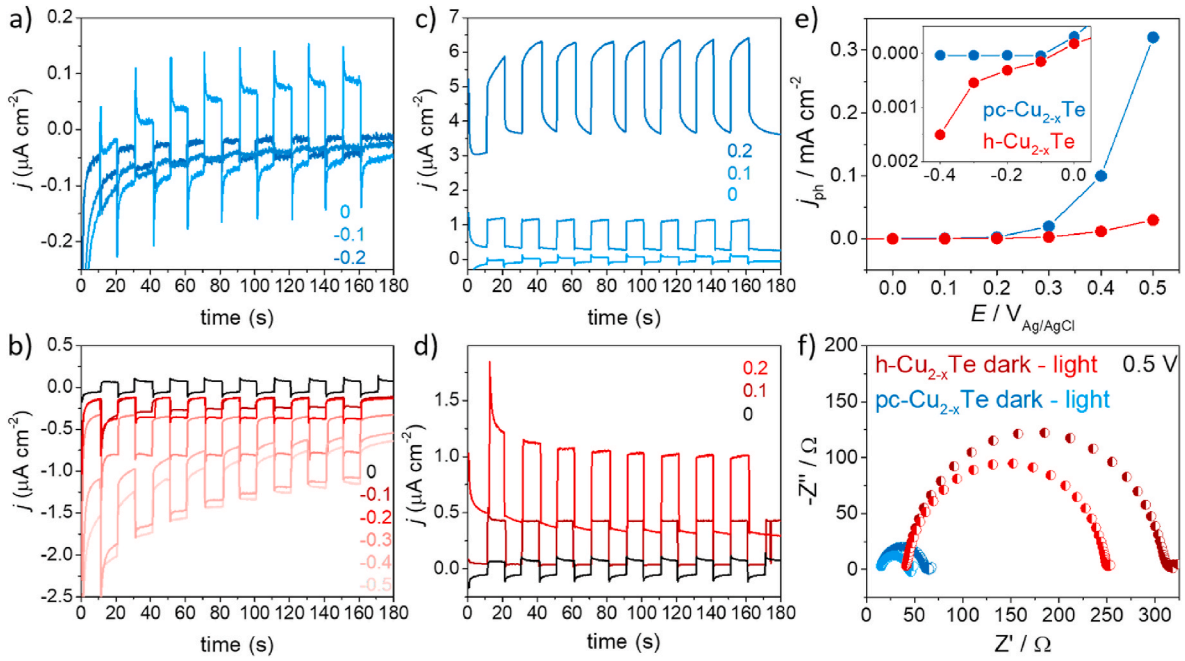

Fig. 3. a-d) Chronoamperometries under chopped AM1.5G illumination at different bias potentials (V vs Ag/AgCl) of pc-$Cu_{2-x}Te$ (blue, a and c) and h-$Cu_{2-x}Te$ (red, b and d) in 0.5 M Na_2SO_3 and pH 9. e) Extracted photocurrents and f) Nyquist plot obtained under dark and illumination conditions at 0.5 V vs Ag/AgCl of both photoelectrodes. (For interpretation of the references to color in this figure legend, the reader is referred to the Web version of this article.)

visible range), it is often combined with other materials in order to create anodes absorbing a wide region of the solar spectrum [43,44]. Furthermore, due to the electronic position of its valence and conduction bands with respect to pc-$Cu_{2-x}Te$ can behave as an electron selective layer (ESL) that prevents electronic recombination. On the other hand, in order to hinder the slight charge recombination exhibited by h-$Cu_{2-x}Te$ NCs, we decided to combine it with CuI, which is known to be a good hole selective layer (HSL) but limited light abortion range.[19–21] This configuration will allow to improve the charge transfer and therefore the efficiency of the photocathode.

Before building the monolithic tandem PEC cell, each hybrid photoelectrode was characterized separately and compared to their single components in order to quantify possible and desired synergistic effects. The results acquired through LSV under chopped illumination (Fig. 4a and b) show that: i) both the dark and photocurrent of the pc-$Cu_{2-x}Te$/TiO_2 hybrid photoelectrode is one and two orders of magnitude higher than those of bare TiO_2 or pc-$Cu_{2-x}Te$ ones, respectively (Fig. 3 a); ii) the photocurrent of the hybrid h-$Cu_{2-x}Te$/CuI photocathode is three orders of magnitude higher than those of CuI and h-$Cu_{2-x}Te$ (Fig. 3b). To confirm this behavior, we performed chronoamperometries at different

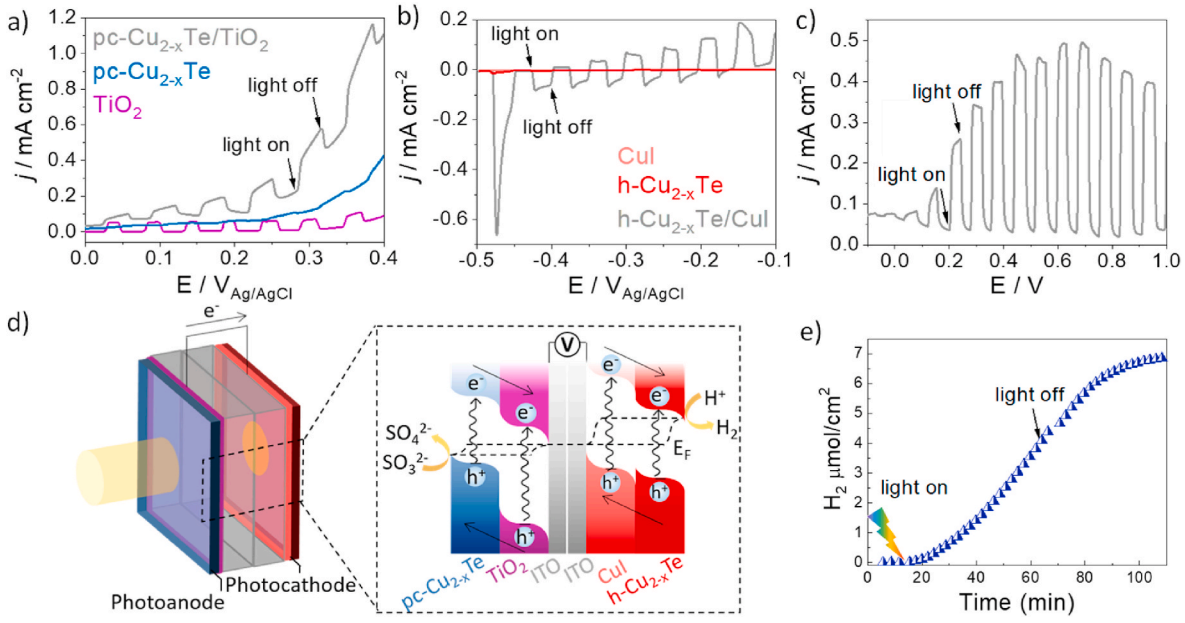

Fig. 4. LSV under chopped AM1.5G illumination of the hybrid photoanode (a) and photocathode (b) compared to their separated components in a three-electrode configuration. LSV (c), scheme (d) and accumulated H_2 evolution at 0.6 V (e) of the monolithic tandem PEC cell in a two-electrode configuration under AM1.5G illumination in 0.5 M Na_2SO_3 electrolyte.

bias potentials, demonstrating the improvement in light absorption and charge transfer in both photoelectrodes (Fig. S10). However, this improvement cannot be attributed to a reduced recombination in the case of the h-$Cu_{2-x}Te$/CuI hybrid photocathode, which still shows recombination at very negative potentials (Fig. 4b and S14).

Encouraged by these results, we built a monolithic tandem PEC cell (Fig. 4d and S15b) and measured the performance in both three- (Fig. S16) and two-electrode (Fig. 4c) configurations. In this sense, results with three electrodes demonstrate that this cell has the potential to harvest the solar energy and transfer it to the external circuit. The recorded photocurrents are around 0.2 mA/cm^2 in a wide range of potential.

In light of these results, we moved to a two-electrode configuration to understand the real potential difference between the two photoelectrodes and afterwards performed HER experiments. In Fig. 4c, the onset potential appears at −0.1 V, and photocurrents reach values of around 0.5 mA/cm^2 at 0.6 V. The HER experiments were preformed depositing a thin film of Pt (17 nm, see the AFM profile in Fig. S17) over the h-$Cu_{2-x}Te$ as co-catalyst. To do this, a flow of argon was passed through the photoelectrochemical cell and it was connected to a gas chromatograph that allows on-line measurements. The accumulated H_2 generated after 1 h of AM 1.5G irradiance was 7 μmol at 0.6 V (Fig. 3d) and the photocurrent reached 1 mA/cm^2 (Fig. S18). Finally, the Faradaic efficiency (η_F) and the applied bias photon-to-current efficiency (ABPE) taking into account the applied bias, V_b, and the sacrificial agent oxidation potential [45] were calculated (more details in S.I), revealing a η_F maximum of 40% and a ABPE of 0.025% (Fig. S 19).

4- Conclusions

To conclude, in this work we have successfully designed and built a tandem PEC cell, that covers a wide part of the solar spectrum, by using two hybrid photoelectrodes based on hexagonal and pseudo-cubic $Cu_{2-x}Te$ crystalline phases, exhibiting different structural and optoelectronic properties. On one hand, pc-$Cu_{2-x}Te$ was selected to build the photoanode, due to its higher positive photocurrents, and combined with TiO_2 as a UV light absorber and electron scavenger. This hybrid photoanode shows synergic increase of one and two orders of magnitude in the photocurrent compared to the single components. On the other hand, by h-$Cu_{2-x}Te$ was selected for the photocathode and combined with CuI as light absorber and hole scavenger. This hybrid photocathode shows an enhancement of the photocurrents of three orders of magnitude with respect to both single materials. The tandem cell was tested in a 1-h H_2 evolution experiment and produced a total of 7 μmol of H_2 with a photocurrent of 1 mA/cm^2 and no signs of aging.

Associated content

Supporting information

FTIR spectra, EIS measurements and data obtained by fitting, HT-XRD of $Cu_{2-x}Te$ NCs, XPS analysis of pc-$Cu_{2-x}Te$ and h-$Cu_{2-x}Te$ photoelectrodes, FESEM images, microanalysis and cross section of the photoelectrodes, UV-VIS-NIR spectroscopy measurements, additional photoelectrochemical characterization, AFM analysis of Pt thin film, pictures of the PEC setup and the photoelectrodes.

CRediT authorship contribution statement

Elena Alfonso-González: Writing – original draft, Methodology, Investigation, Formal analysis, Data curation, Conceptualization. **Marta Liras:** Writing – review & editing, Methodology, Funding acquisition. **Mengjiao Wang:** Methodology, Investigation. **Ignacio J. Villar-García:** Writing – review & editing, Formal analysis, Data curation. **Luca de Trizio:** Writing – review & editing, Methodology. **Mariam Barawi:** Supervision, Investigation, Formal analysis, Data curation, Conceptualization, Funding acquisition, Writing - original draft, Writing - review & editing. **Victor A. de la Peña O'Shea:** Writing – review & editing, Supervision, Investigation, Funding acquisition, Conceptualization.

Declaration of competing interest

The authors declare that they have no known competing financial interests or personal relationships that could have appeared to influence the work reported in this paper.

Data availability

Data will be made available on request.

Acknowledgments

This work was supported by the national projects NovaCO2 (PID2020-118593RB-C22) and Nhympha (PID2019-106315RB-I00) funded by MCIN/AEI/10.13039/501100011033 and the regional project FotoArt-CM (S2018/NMT-4367) funded by Comunidad de Madrid. M.B. thanks the Spanish MCIN the *Juan de la Cierva Incorporación* grant (IJC2019 – 042430 –I). We gratefully acknowledge Fernando Picó for the XRD measurements. The results reflect only the authors' view and the Agency is not responsible for any use that may be made of the information they contained.

Appendix A. Supplementary data

Supplementary data to this article can be found online at https://doi.org/10.1016/j.solmat.2022.112050.

References

[1] J.H. Kim, D. Hansora, P. Sharma, J.W. Jang, J.S. Lee, Toward practical solar hydrogen production-an artificial photosynthetic leaf-to-farm challenge, Chem. Soc. Rev. 48 (2019), https://doi.org/10.1039/c8cs00699g, 1908–1971.
[2] N.S. Lewis, D.G. Nocera, Powering the planet: chemical challenges in solar energy utilization, Proc. Natl. Acad. Sci. U. S. A 103 (43) (2006) 15729–15735, https://doi.org/10.1073/pnas.0710559104. DOI:10.1073/pnas.0603395103), Proceedings of the National Academy of Sciences of the United States of America. 103 (2006) 15729–15735.
[3] K. Sivula, R. van de Krol, Semiconducting materials for photoelectrochemical energy conversion, Nat. Rev. Mater. 1 (2016) 1–16, https://doi.org/10.1038/natrevmats.2015.10.
[4] J.L. Young, M.A. Steiner, H. Döscher, R.M. France, J.A. Turner, T.G. Deutsch, Direct solar-to-hydrogen conversion via inverted metamophic multijunction semiconductor architectures, Nat. Energy 2 (2017) 1–8, https://doi.org/10.1038/nenergy.2017.28.
[5] C. Li, J. He, Y. Xiao, Y. Li, J.J. Delaunay, Earth-abundant Cu-based metal oxide photocathodes for photoelectrochemical water splitting, Energy Environ. Sci. 13 (2020) 3269–3306, https://doi.org/10.1039/d0ee02397c.
[6] Y. Yang, S. Niu, D. Han, T. Liu, G. Wang, Y. Li, Progress in developing metal oxide nanomaterials for photoelectrochemical water splitting, Adv. Energy Mater. 7 (2017) 1–26, https://doi.org/10.1002/aenm.201700555.
[7] K. Sivula, Metal oxide photoelectrodes for solar fuel production, surface traps, and catalysis, J. Phys. Chem. Lett. 4 (2013) 1624–1633, https://doi.org/10.1021/jz4002983.
[8] K. Sivula, F. Le Formal, M. Grätzel, Solar water splitting: progress using hematite (α-Fe 2O3) photoelectrodes, ChemSusChem 4 (2011) 432–449, https://doi.org/10.1002/cssc.201000416.
[9] S. Chandrasekaran, L. Yao, L. Deng, C. Bowen, Y. Zhang, S. Chen, Z. Lin, F. Peng, P. Zhang, Recent advances in metal sulfides: from controlled fabrication to electrocatalytic, photocatalytic and photoelectrochemical water splitting and beyond, Chem. Soc. Rev. 48 (2019) 4178–4280, https://doi.org/10.1039/c8cs00664d.
[10] M.R. Gao, Y.F. Xu, J. Jiang, S.H. Yu, Nanostructured metal chalcogenides: synthesis, modification, and applications in energy conversion and storage devices, Chem. Soc. Rev. 42 (2013) 2986–3017, https://doi.org/10.1039/c2cs35310e.
[11] T. Hisatomi, J. Kubota, K. Domen, Recent advances in semiconductors for photocatalytic and photoelectrochemical water splitting, Chem. Soc. Rev. 43 (2014) 7520–7535, https://doi.org/10.1039/c3cs60378d.
[12] W. Yang, R.R. Prabhakar, J. Tan, S.D. Tilley, J. Moon, Strategies for enhancing the photocurrent, photovoltage, and stability of photoelectrodes for photoelectrochemical water splitting, Chem. Soc. Rev. 48 (2019) 4979–5015, https://doi.org/10.1039/c8cs00997j.

[13] J. Jian, G. Jiang, R. van de Krol, B. Wei, H. Wang, Recent advances in rational engineering of multinary semiconductors for photoelectrochemical hydrogen generation, Nano Energy (2018), https://doi.org/10.1016/j.nanoen.2018.06.074.
[14] R. van de Krol, M. Grätzel, Photoelectrochemical Hydrogen Production, 2012, https://doi.org/10.1007/978-1-4614-1380-6.
[15] S. Giménez, J. Bisquert (Eds.), Photoelectrochemical Solar Fuel Production. From Basic Principles to Advanced Devices, 2016.
[16] L. Jin, H. Zhao, Z.M. Wang, F. Rosei, Quantum dots: quantum dots-based photoelectrochemical hydrogen evolution from water splitting (adv. Energy mater. 12/2021), Adv. Energy Mater. 11 (2021), 2170047, https://doi.org/10.1002/aenm.202170047.
[17] R.H. Gonçalves, B.H.R. Lima, E.R. Leite, Magnetite colloidal nanocrystals: a facile pathway to prepare mesoporous hematite thin films for photoelectrochemical water splitting, J. Am. Chem. Soc. 133 (2011) 6012–6019, https://doi.org/10.1021/ja111454f.
[18] J. Brillet, M. Grätzel, K. Sivula, Decoupling feature size and functionality in solution-processed, porous hematite electrodes for solar water splitting, Nano Lett. 10 (2010) 4155–4160, https://doi.org/10.1021/nl102708c.
[19] K. Sivula, R. Zboril, F. Le Formal, R. Robert, A. Weidenkaff, J. Tucek, J. Frydrych, M. Grätzel, Photoelectrochemical water splitting with mesoporous hematite prepared by a solution-based colloidal approach, J. Am. Chem. Soc. 132 (2010) 7436–7444, https://doi.org/10.1021/ja101564f.
[20] R. van de Krol, M. Grätzel, Photoelectrochemical Hydrogen Production, Springer, 2012.
[21] C. Coughlan, M. Ibáñez, O. Dobrozhan, A. Singh, A. Cabot, K.M. Ryan, Compound copper chalcogenide nanocrystals, Chem. Rev. 117 (2017) 5865–6109, https://doi.org/10.1021/acs.chemrev.6b00376.
[22] C. Grimes, O. Varghese, S. Ranjan, Light, Water, Hydrogen: the Solar Generation of Hydrogen by Water Photoelectrolysis, Springer, 2007, https://doi.org/10.1007/978-0-387-68238-9.
[23] U.V. Ghorpade, M.P. Suryawanshi, S.W. Shin, J. Kim, S.H. Kang, J.S. Ha, S. S. Kolekar, J.H. Kim, Unassisted visible solar water splitting with efficient photoelectrodes sensitized by quantum dots synthesized: via an environmentally friendly eutectic solvent-mediated approach, J. Mater. Chem. 6 (2018) 22566–22579, https://doi.org/10.1039/c8ta05901b.
[24] M. Arunachalam, Y. Jun Seo, S. Jeon, K.S. Ahn, C. Soo Kim, S. Hyung Kang, Colloidal metal Ag nanowire as an efficient co-catalyst for enhancing the solar water oxidation of fluorinated BiVO4 photoelectrode, Chem. Eng. J. 394 (2020), 125016, https://doi.org/10.1016/j.cej.2020.125016.
[25] M.S. Prévot, K. Sivula, Photoelectrochemical tandem cells for solar water splitting, J. Phys. Chem. C 117 (2013) 17879–17893.
[26] G. Xie, K. Zhang, B. Guo, Q. Liu, L. Fang, J.R. Gong, Graphene-based materials for hydrogen generation from light-driven water splitting, Adv. Mater. 25 (2013) 3820–3839, https://doi.org/10.1002/adma.201301207.
[27] A. Naldoni, T. Montini, F. Malara, M.M. Mróz, A. Beltram, T. Virgili, C.L. Boldrini, M. Marelli, I. Romero-Ocaña, J.J. Delgado, V. Dal Santo, P. Fornasiero, Hot electron collection on brookite nanorods lateral facets for plasmon-enhanced water oxidation, ACS Catal. (2017) 1270–1278, https://doi.org/10.1021/acscatal.6b03092.
[28] S.Y. Tee, K.Y. Win, W.S. Teo, L.-D. Koh, S. Liu, C.P. Teng, M.-Y. Han, Recent progress in energy-driven water splitting, Adv. Sci. (2017), 1600337, https://doi.org/10.1002/advs.201600337.
[29] M. Barawi, E. Flores, I.J. Ferrer, J.R. Ares, C. Sánchez, Titanium trisulphide (TiS 3) nanoribbons for easy hydrogen photogeneration under visible light, J. Mater. Chem. A. 3 (2015) 7959–7965, https://doi.org/10.1039/C5TA00192G.
[30] E. Mugnaioli, M. Gemmi, R. Tu, J. David, G. Bertoni, R. Gaspari, L. De Trizio, L. Manna, Ab initio structure determination of Cu2- xTe plasmonic nanocrystals by precession-assisted electron diffraction tomography and HAADF-STEM imaging, Inorg. Chem. 57 (2018) 10241–10248, https://doi.org/10.1021/acs.inorgchem.8b01445.
[31] S. Kumaravel, K. Karthick, P. Thiruvengetam, J.M. Johny, S.S. Sankar, S. Kundu, Tuning Cu overvoltage for a copper-telluride system in electrocatalytic water reduction and feasible feedstock conversion: a new approach, Inorg. Chem. 59 (2020) 11129–11141, https://doi.org/10.1021/acs.inorgchem.0c01648.
[32] L. Yu, K. Luo, S. Chen, C.G. Duan, Cu-deficiency induced structural transition of Cu2-xTe, CrystEngComm 17 (2015) 2878–2885, https://doi.org/10.1039/c4ce02370f.
[33] J.U. Salmón-Gamboa, A.H. Barajas-Aguilar, L.I. Ruiz-Ortega, A.M. Garay-Tapia, S. J. Jiménez-Sandoval, Vibrational and electrical properties of Cu2-xTe films: experimental data and first principle calculations, Sci. Rep. 8 (2018) 1–12, https://doi.org/10.1038/s41598-018-26461-x.
[34] R. Tu, Y. Xie, G. Bertoni, A. Lak, R. Gaspari, A. Rapallo, A. Cavalli, L. De Trizio, L. Manna, Influence of the ion coordination number on cation exchange reactions with copper telluride nanocrystals, J. Am. Chem. Soc. 138 (2016) 7082, https://doi.org/10.1021/jacs.6b02830. –7090.
[35] S. Tokumitsu, Method for Production of Fineparticle and Method for Production of Indium Organocarboxylate, 2009.
[36] G. Kresse, J. Hafner, Ab initio molecular dynamics for liquid metals, Phys. Rev. B 47 (1993) 558–561, https://doi.org/10.1103/PhysRevB.47.558.
[37] G. Kresse, J. Furthmüller, Efficiency of ab-initio total energy calculations for metals and semiconductors using a plane-wave basis set, Comput. Mater. Sci. 6 (1996) 15–50, https://doi.org/10.1016/0927-0256(96)00008-0.
[38] J.P. Perdew, K. Burke, M. Ernzerhof, Generalized gradient approximation made simple, Phys. Rev. Lett. 77 (1996) 3865–3868, https://doi.org/10.1103/PhysRevLett.77.3865.
[39] J. Heyd, G.E. Scuseria, M. Ernzerhof, Hybrid functionals based on a screened Coulomb potential, J. Chem. Phys. 118 (2003) 8207–8215, https://doi.org/10.1063/1.1564060.
[40] F. Cardon, W.P. Gomes, On the determination of the flat-band potential of a semiconductor in contact with a metal or an electrolyte from the Mott-Schottky plot, J. Phys. Appl. Phys. 11 (1978), https://doi.org/10.1088/0022-3727/11/4/003.
[41] S. Kment, F. Riboni, S. Pausova, L. Wang, L. Wang, H. Han, Z. Hubicka, J. Krysa, P. Schmuki, R. Zboril, Photoanodes based on TiO2 and α-Fe2O3 for solar water splitting-superior role of 1D nanoarchitectures and of combined heterostructures, Chem. Soc. Rev. 46 (2017) 3716–3769, https://doi.org/10.1039/c6cs00015k.
[42] A. El Ruby Mohamed, S. Rohani, Modified TiO2 nanotube arrays (TNTAs): progressive strategies towards visible light responsive photoanode, a review, Energy Environ. Sci. 4 (2011) 1065–1086, https://doi.org/10.1039/c0ee00488j.
[43] X. Chen, Z. Zhang, L. Chi, A.K. Nair, W. Shangguan, Z. Jiang, Recent advances in visible-light-driven photoelectrochemical water splitting: catalyst nanostructures and reaction systems, Nano-Micro Lett. 8 (2016) 1–12, https://doi.org/10.1007/s40820-015-0063-3.
[44] E. Kalamaras, M.M. Maroto-Valer, M. Shao, J. Xuan, H. Wang, Solar carbon fuel via photoelectrochemistry, Catal. Today 317 (2018) 56–75, https://doi.org/10.1016/j.cattod.2018.02.045.
[45] Z. Chen, T.F. Jaramillo, T.G. Deutsch, A. Kleiman-Shwarsctein, A.J. Forman, N. Gaillard, R. Garland, K. Takanabe, C. Heske, M. Sunkara, E.W. McFarland, K. Domen, E.L. Milled, H.N. Dinh, Accelerating materials development for photoelectrochemical hydrogen production: standards for methods, definitions, and reporting protocols, J. Mater. Res. 25 (2010) 3–16, https://doi.org/10.1557/jmr.2010.0020.